CHAPTER-III

SLIME BASED WIDE-BAND META-STRUCTURE ABSORBER WITH DUAL RESONATING STRUCTURE

3.1 INTRODUCTION

Single slime-based MSA, investigated in chapter II, showed – 10 dB absorption for 47% of the X-band ranging from 9.54-12.4 GHz. It is, however, desirable for the absorber to cover the entire operating band. One of the ways of achieving wideband functioning MSA is through modifications of the unit cell's overall shape and the design of the resonators [1-3]. Implementing the technique requires rigorous geometrical optimizations followed by fabrication complexity. Another effective way to achieve wideband absorption is to incorporate multi-resonant structures in a unit cell [4-8]. MSAs with multi-resonant structures have two possible configurations: they can be either stacked on top of one another [7, 9-11] or integrated into a co-planar structure [12]. Both the design strategies share the same fundamental element of producing multi-resonance responses that, when coupled, yields a wideband absorption spectrum. Unlike stacked multi-resonant structures, co-planar multi-resonant structures do not add thickness to the absorber and give a planar finish which have added advantage of easy mounting on curved surfaces [7, 10]. Furthermore, the co-planar multi resonant structures are easier to design and optimize as the resonant peaks can be independently manipulated with minimal mutual coupling among the resonators [12]. In contrast, stacked structures requires more geometrical optimization to reduce the mutual coupling among the resonators.

In this chapter, broadening of the absorption bandwidth of the slime based MSA is realized by incorporating dual co-planar embedded resonators in the same unit structure similar to reference [12]. The resonators are symmetrically shaped to absorb EM wave at different polarization angles. Here, two differently shaped resonating structures– cuboidal with four-fold symmetry (4FS) and hexagonal prism with six -fold symmetry (6FS) are used for making the MSAs. Prior to fabrication, the dimensions of the unit cell and the resonating structures are optimized to cover the entire working band. The fabricated MSAs are tested for absorption performance and evaluated for its extent of restoration ability and recovery time.

3.2 DESIGN AND OPTIMIZATION OF WIDE-BANDWIDTH MSAs

Low and high frequency resonating structures are selected so as to resonate at either side of the central frequency of the X- band and thus the overlapping of the absorbing spectra will cover the entire band. The outer dimensions of the two resonating

structures are kept same for easy amalgamation during fabrication. Optimizations are conducted to achieve a comprehensive bandwidth with more than 90% absorption, spanning over the X-band for both cuboidal MSA 4FS-$[L_1L_2]$ and hexagonal-prism MSA 6FS-$[R_1R_2]$.

3.2.1 Geometry of cuboidal MSA unit cell

Two different cuboidal shaped resonating structures, $[L_1]$ resonating at higher frequency and $[L_2]$ resonating at lower frequency are combined to form a unit cell, MSA 4FS-$[L_1L_2]$, drawn in Figure 3.1(a). The parameters, displayed in Figure 3.1(b) and (c), are optimized to cover entire X-band and tabulated in Table 3.1.
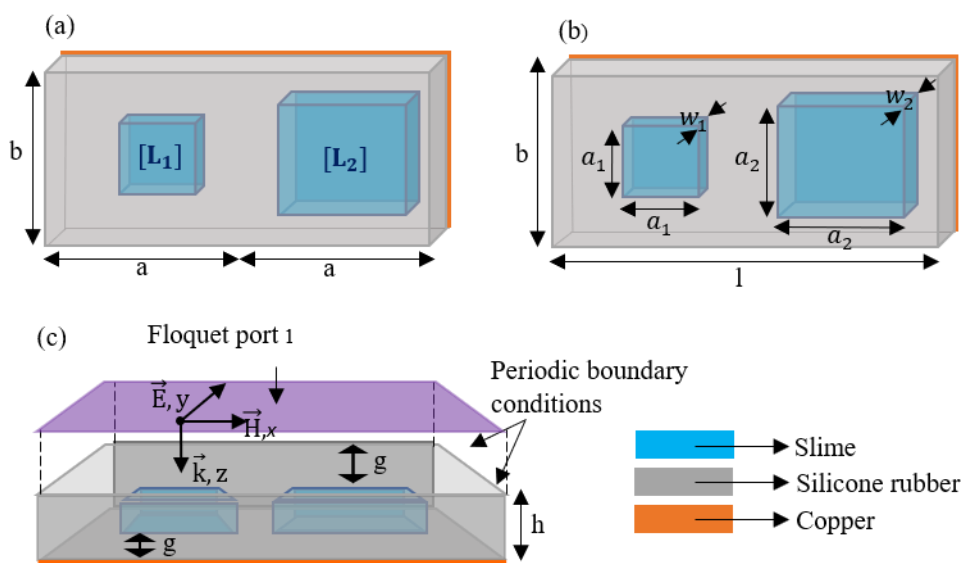
Figure 3.1 Schematic of cuboidal MSA 4FS-[L₁L₂] (a) top view layout of unit cell with external dimensions, (b) top view with structural parameters and (c) side view and simulation setup with Floquet port.

Table 3.1 Optimized parameters of cuboidal MSA.

Parameters	Description	Values (mm)
l=2a	Length of the silicone substrate	24
b	Breadth of the silicone substrate	12
a_1	Length of the cuboidal resonator [L₁]	5
a_2	Length of the cuboidal resonator [L₂]	8
$w_1=w_2$	Height of the MSA 4FS-[L₁L₂]	1
g	Silicone layer thickness below and above slime resonators	1
h	Height of the silicone substrate	3
	Copper tape thickness (metal back)	0.035

The MSA is backed by copper tape.

3.2.2 Geometry of hexagonal-prism MSA unit cell

The unit cell here comprises of hexagonal prism-shaped resonators, [R_1] and [R_2], resonating at higher and lower frequencies of X-band respectively. Hexagonal-prism shaped structure is studied here as the geometry has comparatively smaller total volume with other identical height subwavelength structures resonating at same frequency. The six-fold surface symmetry enables polarization independence over a wider angle. The arrangement and the dimensions of the unit cell, 6FS-[R_1R_2], are given in Figure 3.2(a)-(c). The optimized parameters are given in Table 3.2.
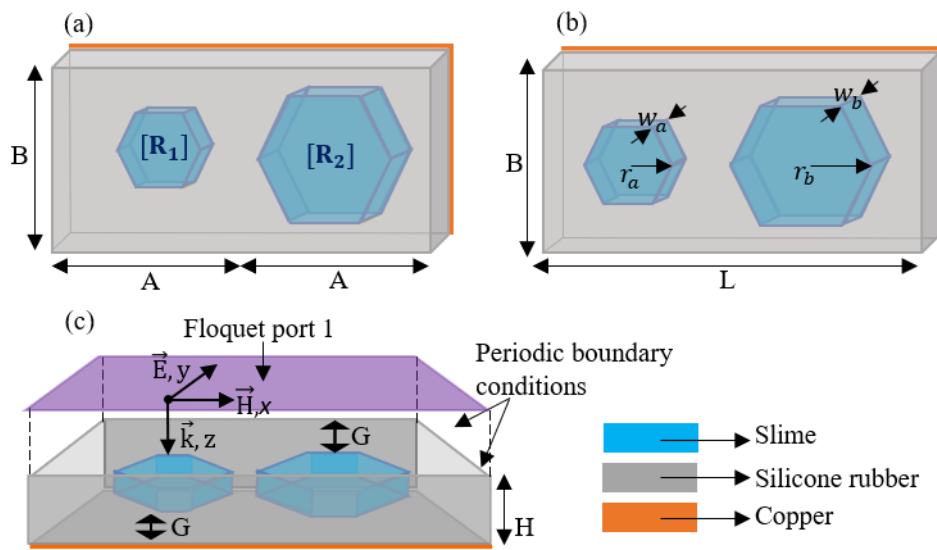
Figure 3.2 Schematic of hexagonal-prism MSA 6FS-[R_1R_2] (a) top view layout of unit cell with external dimensions, (b) top view with structural parameters and (c) side view and simulation setup with Floquet port.

Table 3.2 Optimized parameters of hexagonal-prism MSA.

| Parameters	Description	Value (mm)
L=2A	Length of the substrate	24
B	Breadth of the substrate	12
r_a	Outer radius of the resonator [R_1]	3.4
r_b	Outer radius of the resonator [R_2]	5.2
$w_a=w_b$	Height of the MSA 6FS-[R_1R_2]	1
G	Silicone layer thickness below and above slime resonators	1
H	Height of the substrate	3
	Copper tape thickness (metal back)	0.035

3.3 SIMULATED ABSORPTION CHARACTERISTICS

In simulation, the electromagnetic wave is allowed to incident on the designed absorbers along the z-axis (k-vector), electric (E)-field is along y-axis and magnetic

(H)-field is along x-axis, Figure 3.1(c) and Figure 3.2(c), using Floquet port. The x and y axes of the unit cell are subject to the periodic boundary conditions.
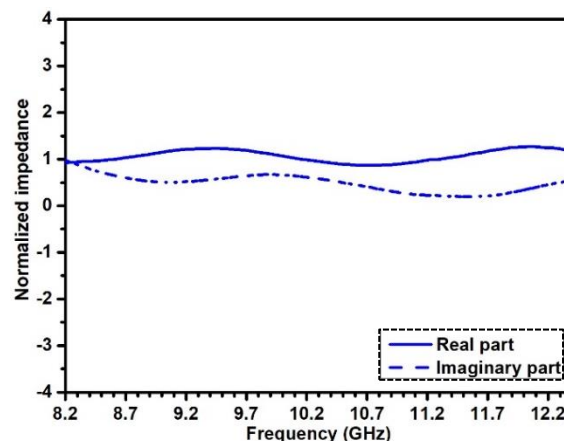
3.3.1 Cuboidal MSA

Figure 3.3(a) plots the reflection loss values and corresponding absorbance at normal incidence. A wide -10 dB bandwidth of 3.8 GHz with [L_1] resonating at 11.43 GHz with reflection loss of -19.8 dB and [L_2] resonating at 9.03 GHz with reflection loss of -12.4 dB is observed. Absorbance is found to be >90% over almost the entire bandwidth, Figure 3.3(b), which is determined using equation (2.3).
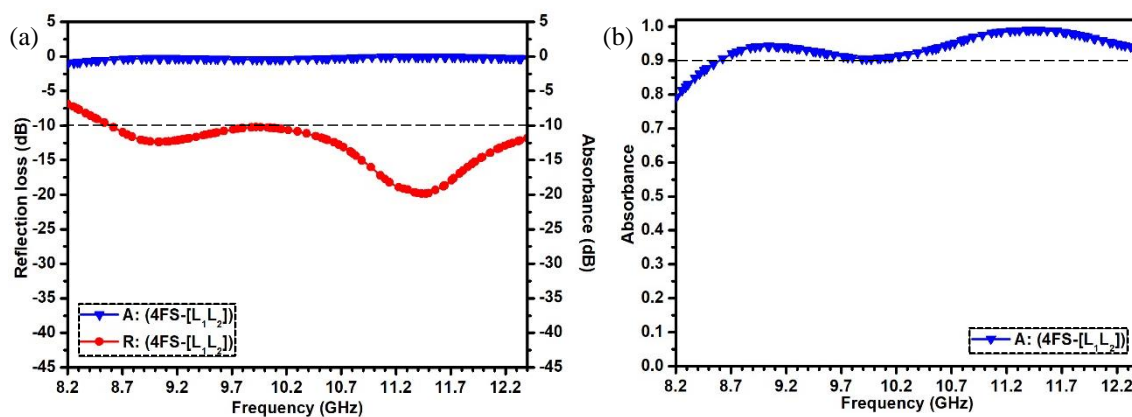
Figure 3.3 (a) Reflection loss values with corresponding absorbance in dB scale and (b) absorbance in linear scale of cuboidal MSA.
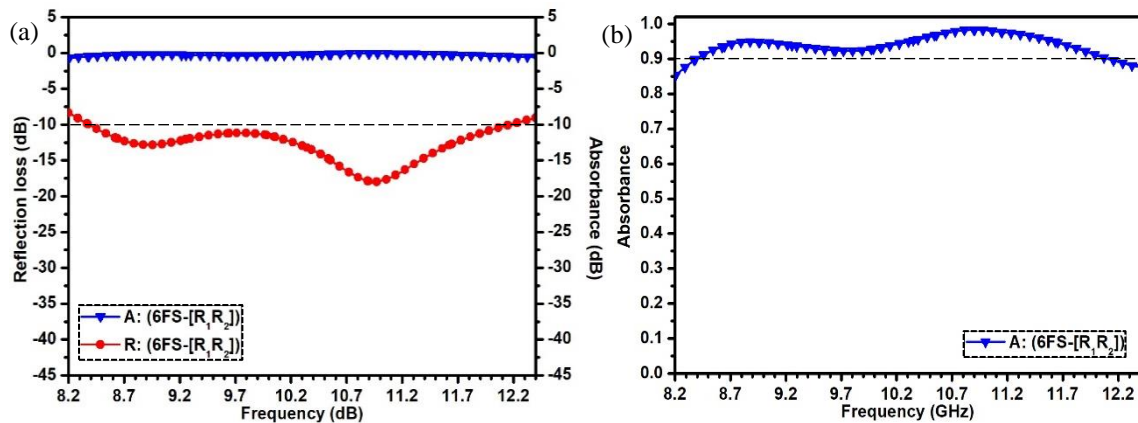
Normalized impedance values of the MSAs at X-band are plotted in Figure 3.4. The real part, $Z_a' \to 1$ while the imaginary part, $Z_a'' \to 0$ almost throughout the band indicating broadband impedance matching.

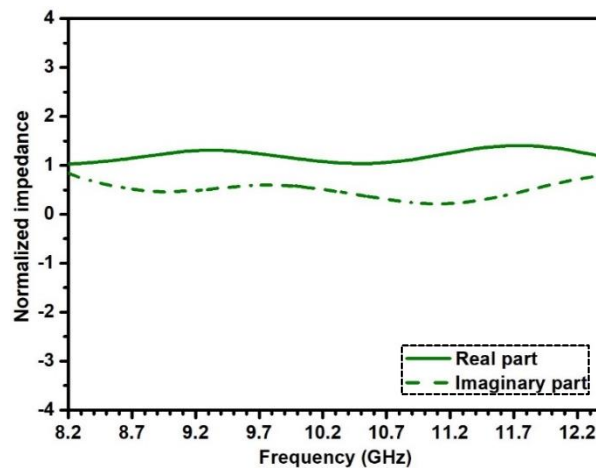**Figure 3.4** Simulated normalized impedance of cuboidal MSA.

3.3.2 Hexagonal-prism MSA

The reflection loss and corresponding absorbance spectra at normal incidence are plotted in Figure 3.5(a). The reflection loss curve shows two resonance peaks at 8.95 GHz and 10.97 GHz with reflection loss of -12.83 dB and -17.95 dB, corresponding to $[R_2]$ and $[R_1]$, respectively, and - 10 dB bandwidth coverage is ~3.7 GHz. Absorbance >90% is observed over almost the entire band, Figure 3.5(b).

Figure 3.5 (a) Reflection loss values with corresponding absorbance in dB scale and (b) absorbance in linear scale of hexagonal-prism MSA.

Figure 3.6 displays the normalized impedance values of the MSA at X-band. Broadband impedance matching condition is achieved with $Z_a' \rightarrow 1$ and $Z_a'' \rightarrow 0$.


Figure 3.6 Simulated normalized impedance of hexagonal-prism MSA.

3.3.3 Field distribution analysis

Comprehensive analysis of vector field distribution is conducted to comprehend the absorption mechanism at resonance peaks.

Cuboidal MSA: Field analysis is carried out at the two dominant resonance frequencies, Figure 3.7. The distribution of the fields show similar pattern as observed in the previous chapter, section 2.4 with E-field concentrated at the edges and magnetic field confined within the slime resonators. The scattered power is located in the lossy slime resonators. The field patterns confirm dual resonance with [L$_1$] resonating at 11.43 GHz and [L$_2$] at 9.03 GHz. The coupling eventually leads to bandwidth broadening.
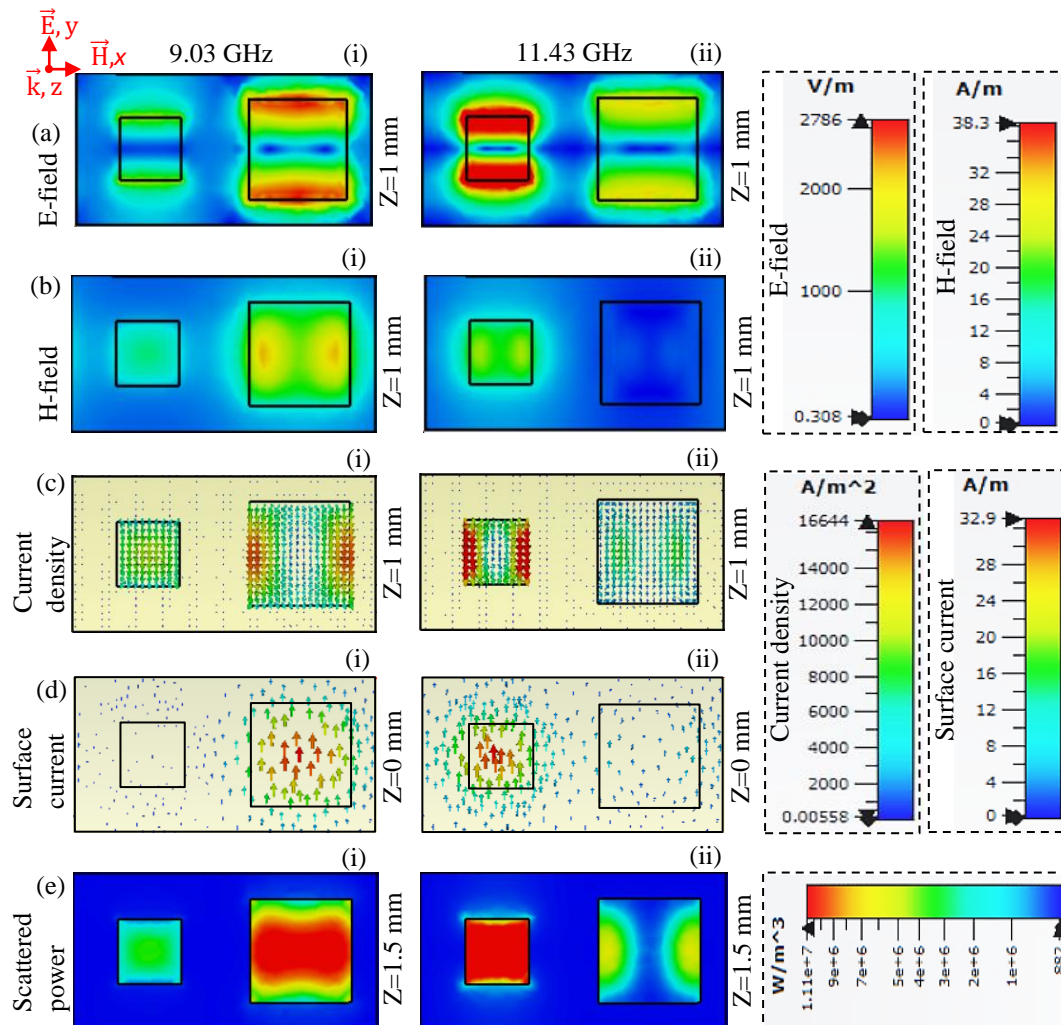
Figure 3.7 (a) E-field distribution, (b) H-field distribution, (c) induced current density, (d) surface current on the metallic ground plate and (e) scattered power distribution of cuboidal MSA at frequency 9.03 GHz and 11.43 GHz.

Hexagonal MSA: Field analysis is carried out for hexagonal-prism MSA, Figure 3.8, for [R$_1$] and [R$_2$] at their respective resonating frequencies viz. 10.9 GHz and 8.8 GHz. The E-field, H-field, induced current density, surface currents and the scattered power showed similar distribution.
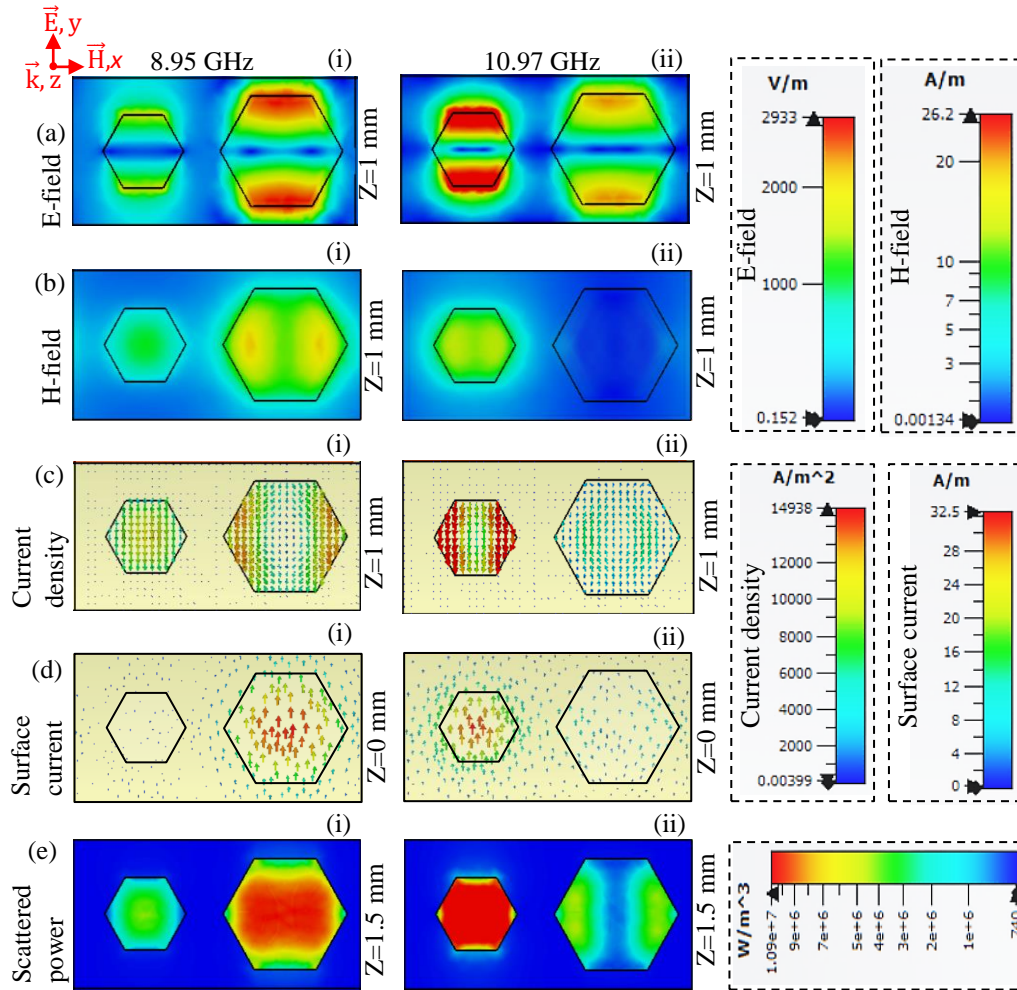
Figure 3.8 (a) E-field distribution, (b) H-field distribution, (c) induced current density, (d) surface current at the metallic ground plate and (e) scattered power distribution of hexagonal-prism MSA at frequency 8.95 GHz and 10.97 GHz.

3.4 MEASURED ABSORPTION CHARACTERISTICS

The absorber samples are fabricated using optimized dimensions from Table 3.1 and 3.2. Subsequently, the absorption performance of the developed absorber samples is measured.

3.4.1 Fabrication of the wide-bandwidth MSAs

The in lab fabricated MSAs are sized to 22.86 × 10.16 mm^2 to fit in the waveguide kit. The fabrication is carried out likewise as mentioned in chapter II, section 2.5.1. Figure 3.9 represents different stages of the fabricated MSA samples.
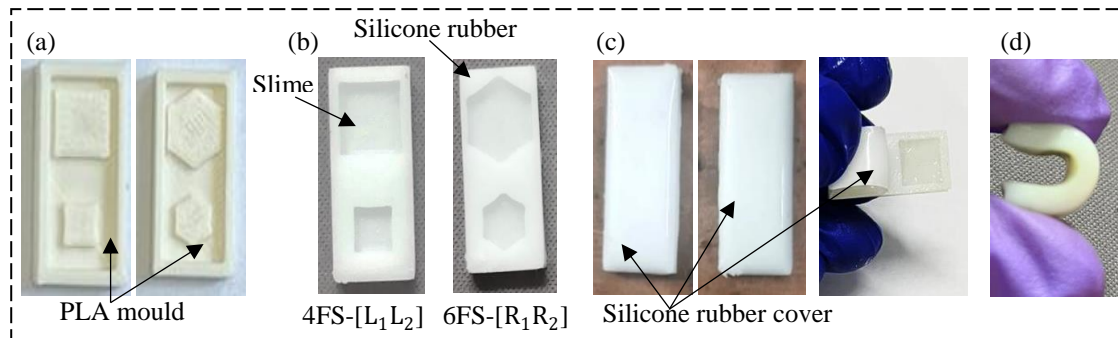
Figure 3.9 Fabrication of cuboidal MSA and hexagonal-prism MSA. (a) 3D printed molds, (b) silicone substrates with grooves filled with slime and (c) sealed final product. (d) Demonstration of flexibility of the fabricated MSA.

3.4.2 Absorption performance

The samples are placed at one end of the waveguide (Model WR-90X11644A), Figure 3.10, that is compatible with the Vector Network Analyzer (Model-E8362), the measurement technique detailed in section 2.5.2.
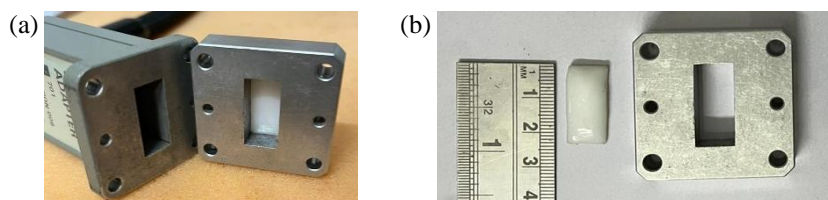
Figure 3.10 MSA (a) mounted inside waveguide kit and (b) alongwith open aperture of waveguide kit.

Cuboidal MSA: The MSA is found to show two distinctive notches of -15.47 dB at 8.7 GHz and -26.4 dB at 11.3 GHz with a -10 dB reflection loss bandwidth of 4.2 GHz, Figure 3.11(a). The entire X-band exhibits an absorption of greater than 90%, Figure 3.11(b).
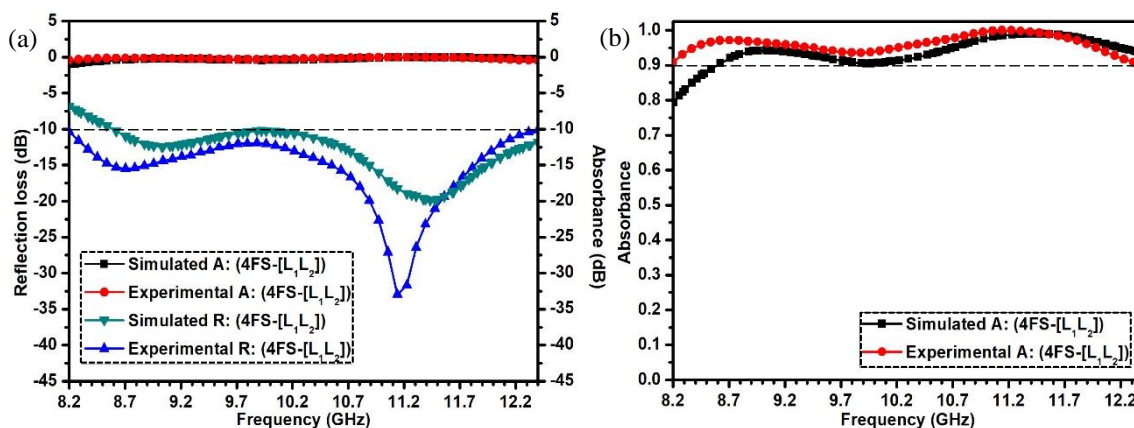
Figure 3.11 Measured and simulated values of (a) reflection loss with corresponding absorbance in dB scale and (b) absorbance in linear scale, of cuboidal MSA.

Hexagonal- prism MSA: The developed MSA has a reflection loss of -17 dB at 8.4 GHz and a loss of -28.9 dB at 10.9 GHz, with a -10 dB bandwidth of 3.8 GHz, as shown in Figure 3.12(a). Absorption >90% is achieved for more than 90% of the X-band as can be observed in Figure 3.12(b).
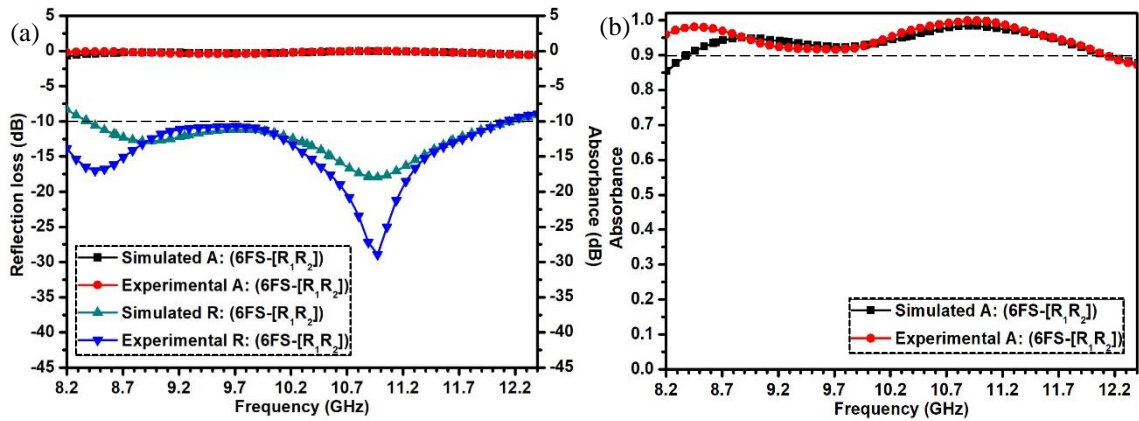
Figure 3.12 Measured and simulated values of (a) reflection loss with corresponding absorbance in dB scale and (b) absorbance in linear scale, of hexagonal-prism MSA.

The simulated and experimental absorption results are tabulated in Table 3.3.

Table 3.3 Absorption results.

Absorber	Cuboidal MSA		Hexagonal-prism MSA	
	Simulated	*Experimental*	*Simulated*	*Experimental*
A_ω >90% BW (GHz)	3.8	4.2	3.7	3.8
% coverage of X-band	90	100	88	90

The contributions of van der Waals forces within the slime molecules are not considered in the simulated results. Further, simulations are carried out using Frequency Solver Domain which is based on Finite Element Method (FEM) that divides a continuous surface into discrete finite elements or meshes and solves polynomial equations at the nodes. A tradeoff between the mesh size and processing time is made in order to achieve the result which may not necessarily consider microscopic variation in the MSA design that may exists in real, hence the disparity, as observed in Table. 3.3.

3.5 REVERTIBILITY EVALUATION
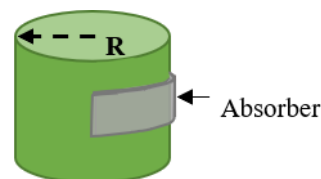
**Figure 3.13** Schematic of bending radius.

A study is conducted on recovery time of the MSAs and the extent of bending it can undergo withholding its absorption performance. First, simulations are carried out at different bending curvatures.

Figure 3.13, gives the schematic of the bending curvature, where R is the bending radius. The simulation result gives an idea of maximum bending which can be carried out without effecting the performance of the MSAs. It is observed from the plots in Figures 3.14(a) and (b) that -10 dB bandwidth is almost consistent upto R=10 mm. A gradual increase in reflection loss, is observed as R decreases from 40 mm to 10 mm. For R<10 mm the performance of the absorbers deteriorates drastically. The maximum bending radius limit for the developed absorber prototypes is taken as 10 mm.
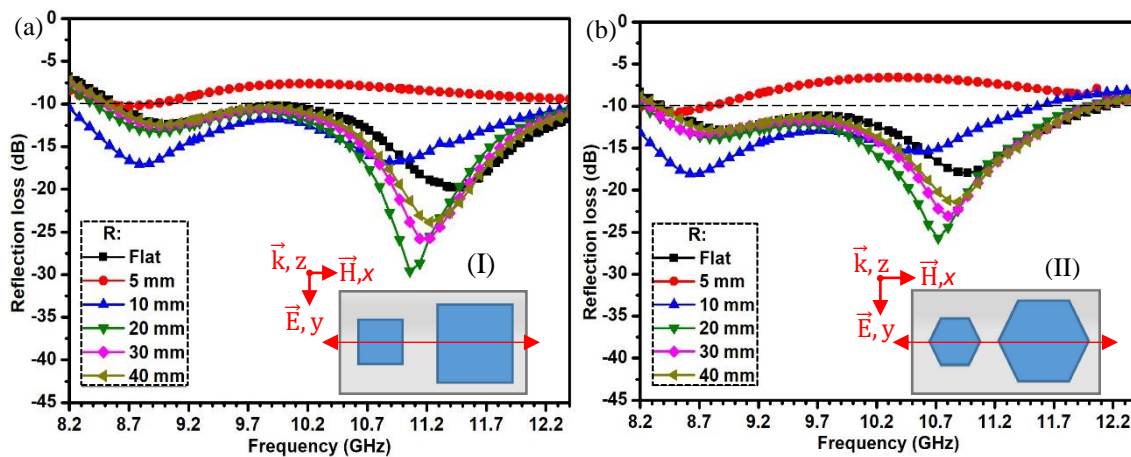
Figure 3.14 Simulated reflection loss values at different bending radii for (a) cuboidal MSA and (b) hexagonal-prism MSA. Inset (I) and (II) showing the bending axis.

A 3D semi-cylindrical support, Figure 3.15(a) for maximum bending, i.e. R=10 mm is printed using BoXZY 3D printer, as shown in Figure 3.15(b). The developed MSA is then placed over the cylindrical surface and is secured to the support with the help of thin parafilm M (from Bemis), Figure 3.15(c).
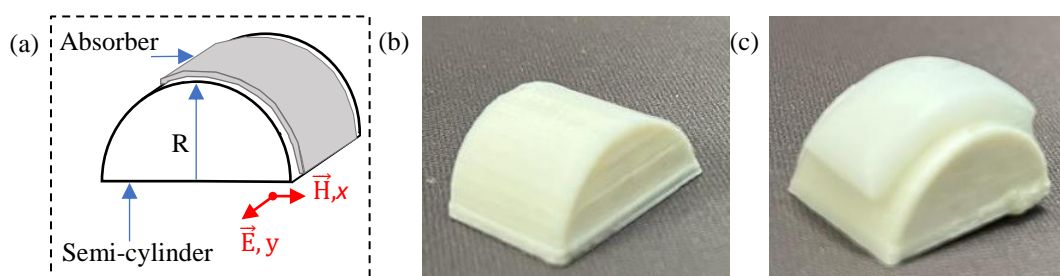
Figure 3.15 Semi-cylindrical structure for R=10 mm (a) schematic and (b) 3D printed support (c) with absorber mounted on top of it.

The prototypes are kept in the position for different time durations, thereafter removed and tested instantly for the absorption performance. It is observed in Figures 3.16(a) and (b) that the -10 dB bandwidth tends to take the values close to the simulated values for 10 mm bending radius, Figures 3.14(a) and (b), when the absorbers are kept in bending position for 14 h which implies that with increase in the time for bending position, the absorbers take a longer time to recover. After 14 h of bending, no appreciable changes in the -10 dB bandwidth is observed even after 24 h of bending. Hence, studies beyond 24 h is not reported.
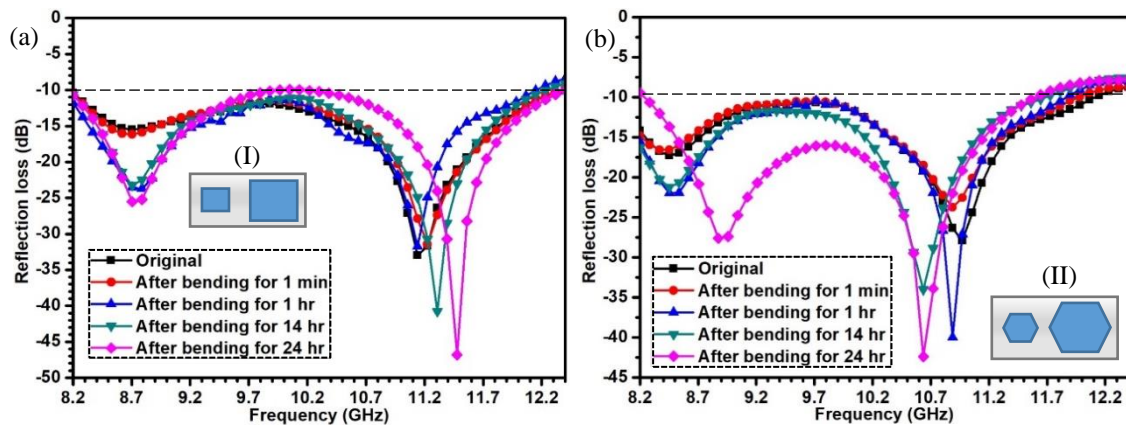

Figure 3.16 Measured reflection values of (a) cuboidal MSA and (b) hexagonal-prism MSA after bending for different time duration.

The recovery duration of the absorber's performance for R=10 mm after 24 h of bending is observed. The prototypes reverted to its original shape instantly with its -10 dB absorption bandwidth almost intact. The original performance of the absorbers, nevertheless, is restored after 15 mins of removal from the bending position as seen in Figure 3.16, for both cuboidal and hexagonal-prism MSAs.
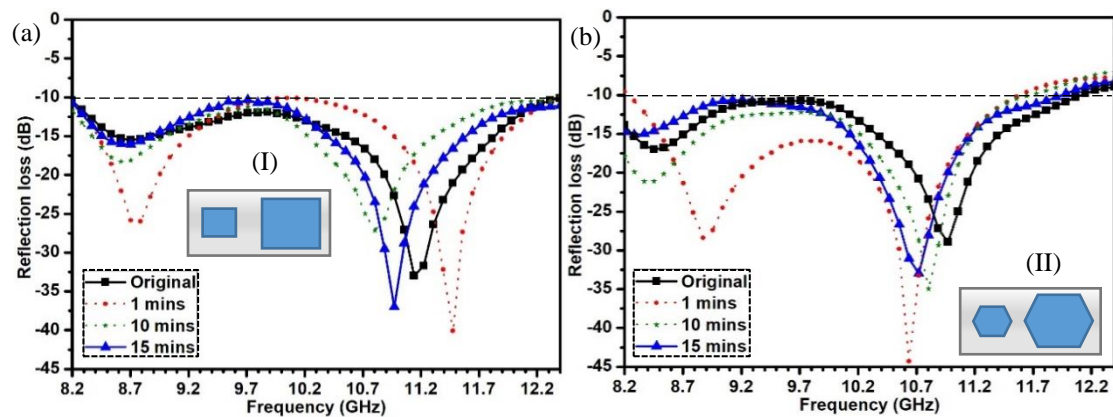
Figure 3.17 Performance recovery in (a) cuboidal MSA and (b) hexagonal-prism MSA.

3.6 ABSORPTION AT DIFFERENT POLARIZATION AND INCIDENT ANGLES

Similar resonators are placed diagonally to develop symmetrical structured MSAs for both cuboidal and hexagonal-prism geometries as drawn in Figures 3.18(a) and (b). Extent of polarization tolerance is studied considering single unit shown in Figures 3.18(c) and (d).
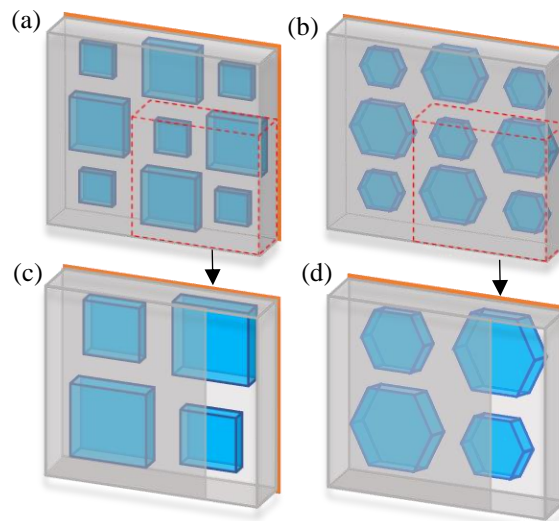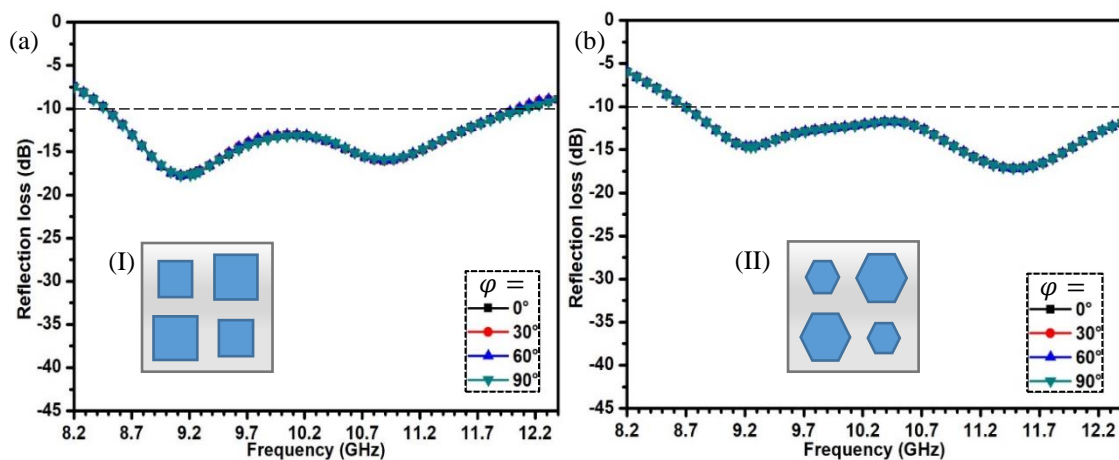

Figure 3.18 (a) Proposed cuboidal MSA and (b) hexagonal-prism MSA and corresponding expanded single unit for (c) cuboidal MSA and (d) hexagonal-prism MSA.

The reflection loss values for different polarization angles (φ) from 0°(co-polarized)−90°(cross-polarized) with a step size of 30 are plotted in Figure 3.19. Interestingly the plots coincided for all the polarization angles revealing polarization independency of the MSAs.

Figure 3.19 Simulated reflection loss values at different polarization angles for (a) cuboidal MSA and (b) hexagonal-prism MSA.

The coupling effect of resonator with ground plane in the unit cell depends on the path length of the EM wave [13, 14]. Path length increases with increase in incident angles (θ). The -10 dB bandwidth reduces as the incident angles varies from 0°-40°, as shown in the plots in Figures 3.19(a)-(d).

The cuboidal MSA is limited upto $\pm 20°$ of incident angle (θ) for both TE and TM modes, Figures 3.20(a) and (b) while in the hexagonal-prism MSA, the -10 dB bandwidth decreases beyond $\pm 30°$ of incident angle (θ) for both TE and TM modes, Figures 3.20(c) and (d). The structures interacts differently with electric and magnetic components of the EM wave hence showing variation in reflection loss in TE and TM modes [15].
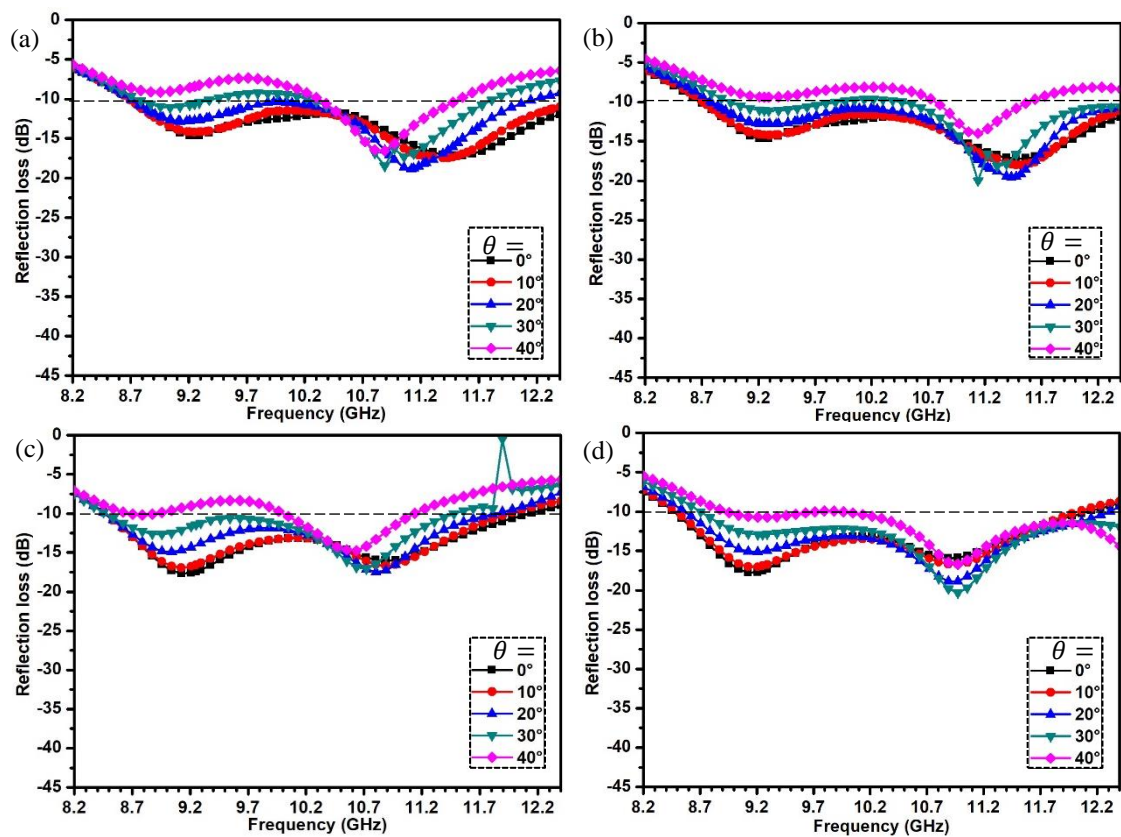
Figure 3.20 Simulated reflection loss values at different incident angles for cuboidal MSA (a) TE mode and (b) TM mode; for hexagonal-prism MSA (c) TE mode and (d) TM mode.

3.7 CHAPTER SUMMARY

This work presents an effective way of enhancing bandwidth through generation of dual resonant peaks with relatively low thickness ($\sim\frac{\lambda}{10}$) slime-based MSAs. Dual resonating structures employed in the MSAs exhibit a broad more than 90%

absorption bandwidth covering almost the entire X-band. The efficacy of the absorber is consistent even after 24 h of bending with bending radius of 10 mm. The MSAs shows performance restoration with a minimum recovery time of ~1 minute and the performance getting completely reverted after ~15 mins. Four-fold (cuboidal) and six-fold (hexagonal-prism) symmetric resonators enable polarization independent absorption. The absorbers are resistant to water, light weighted and revertible finding ample applications in flexible and wearable technology. The performance parameters are summarized in the Table 3.4 below.

Table 3.4 Summary of the absorbers' specifications.

Result→	Experimental					Simulated		
Absorber	**-10 dB BW (GHz)**	**P (mm)**	**Recovery time (Min/Max)**	**WA (%)**	**ρ (g cm^{-3})**	**IA-T**	**PA-T**	**Max Bending radius (mm)**
Cuboidal MSA	4.2 (8.2-12.4)	24×24	1-15 mins	0.6	~1.16	$\pm 20°$	$\pm 90°$	10
Hexagonal-prism MSA	3.8 (8.2-12)	24×24	1-15 mins	0.6	~1.16	$\pm 30°$	$\pm 90°$	10
Note: BW- bandwidth, P-period, Recovery time for 24 h of bending with radius- R=10 mm, WA- absorption= $\frac{Weight_{submergered} - Weight_{actual}}{Weight_{actual}} \times 100$, **ρ**- density, PA-T Polarization angle tolerance, Incidence angle tolerance								

REFERENCES

[1] Zhou, F.-k., et al., An ultra-broadband microwave absorber based on hybrid structure of stereo metamaterial and planar metasurface for the S, C, X and Ku bands. *Results in Physics*, 30: 104811, 2021.

[2] Zhou, Q., et al., A novel lightweight metamaterial with ultra broadband electromagnetic wave absorption induced by three-dimensional CNTs conductive-coated arrays. *Science China Technological Sciences*, 66(3): 881-888, 2023.

[3] Chen, M., et al., Structural design and optimization of double-cross shape broadband absorption metamaterial based on CB-ABS. *Frontiers in Materials*, 9: 980907, 2022.

[4] Wang, G., et al., Design and manufacturing of lightweight modular broadband microwave absorbing metastructure. *Composites Part B: Engineering*, 266: 111007, 2023.

[5] Li, D., et al., Lightweight Metastructure with Broadband Microwave Absorption and Effective Mechanical Resistance Using 3D Printing Technology. *Available at SSRN 4142009*.

[6] Huang, Y., et al., Ultrathin flexible carbon fiber reinforced hierarchical metastructure for broadband microwave absorption with nano lossy composite and multiscale optimization. *ACS applied materials & interfaces*, 10(51): 44731-44740, 2018.

[7] Abdullahi, M. and M. Ali, Additively manufactured metastructure design for broadband radar absorption. *Beni-Suef University Journal of Basic and Applied Sciences*, 10(1): 1-12, 2021.

[8] Huang, Y., et al., Evolutionary optimization design of honeycomb metastructure with effective mechanical resistance and broadband microwave absorption. *Carbon*, 177: 79-89, 2021.

[9] Duan, Y., et al., A wide-angle broadband electromagnetic absorbing metastructure using 3D printing technology. *Materials & Design*, 208: 109900, 2021.

[10]　Zhou, D., X. Huang, and Z. Du, Analysis and design of multilayered broadband radar absorbing metamaterial using the 3-D printing technology-based method. *IEEE Antennas and Wireless Propagation Letters*, 16: 133-136, 2016.

[11]　Song, W.-L., et al., Constructing repairable meta-structures of ultra-broad-band electromagnetic absorption from three-dimensional printed patterned shells. *ACS applied materials & interfaces*, 9(49): 43179-43187, 2017.

[12]　Gogoi, D.J. and N.S. Bhattacharyya, Metasurface absorber based on water meta "molecule" for X-band microwave absorption. *Journal of Applied Physics*, 124(7): 075106, 2018.

[13]　Shuvo, M.M.K., et al., A Wide-Angle, Enhanced Oblique Incidence, Bend-Able Metamaterial Absorber Employed in Visible Region With a Sun Shape Resonator. *IEEE Access*, 9: 126466-126480, 2021.

[14]　Hannan, S., et al., Wide bandwidth angle-and polarization-insensitive symmetric metamaterial absorber for X and Ku band applications. *Scientific Reports*, 10(1): 1-9, 2020.

[15]　Amiri, M., et al., Wide-angle metamaterial absorber with highly insensitive absorption for TE and TM modes. *Scientific reports*, 10(1): 1-13, 2020.